Biophysical Journal Volume 66 April 1994 1104–1114

# Muscle Sound Frequencies of the Frog Are Modulated by Skeletal Muscle Tension

Neil M. Cole* and Daniel T. Barry

Department of Physical Medicine and Rehabilitation and Division of Bioengineering, University of Michigan Medical Center, University Hospital, Ann Arbor, Michigan 48109-0042, and *Institute of Gerontology, University of Michigan, Ann Arbor, Michigan 48109-2007 USA

ABSTRACT The purpose of this study was to determine the relationships among muscle sound frequencies, muscle tension, and stiffness. Time-frequency transformations of nonstationary acoustic signals provided measures of resonant frequency during isometric contractions of frog (Rana pipiens) semitendinosus and gastrocnemius muscles. A mathematical expression for muscle transverse resonant frequency, elastic modulus and tension, based on elastic beam theory, was formulated by the Rayleigh method adapted for muscles. For thin muscles, the elastic modulus was found to have negligible influence on transverse muscle resonant frequency. Changes in muscle tension were the major determinants of changes in transverse resonant frequency. Consequently, for thin muscles, the time course of muscle tension, but not elastic modulus, can be monitored acoustically during the early phase of contraction when muscles give rise to sounds. Muscles were found to be anisotropic with a modulus of elasticity, $E_L$, measured via length perturbations near 0.1% muscle length peak-to-peak, that was much larger than the modulus of elasticity, $E_b$, that resists the lateral bending that causes sound production. The elastic and resonant behavior of a thin muscle is similar to a tensioned fibrous cable with distributed mass.

## INTRODUCTION

Contracting skeletal muscles emit audible pressure waves that are easily recorded with standard microphones (Barry et al., 1985; Oster and Jaffe, 1980). The recording of pressure waves, or muscle sounds, provides a simple, noninvasive, portable measure of the mechanical activity of skeletal muscle. Sounds have been characterized both from skeletal muscles of human beings in vivo and of frogs in vitro. Several clinical applications for muscle sounds exist, including monitoring muscle fatigue (Barry et al., 1985; Barry et al., 1992; Orizio et al., 1989; Zwarts and Keidel, 1991), controlling prosthetic devices (Barry et al., 1986), and diagnosing pediatric muscle disease (Barry et al., 1990). Techniques involving evoked twitches and the use of accelerometers have been developed to obtain muscle vibration data without problems from tremor artifacts or the use of transducer-dependent units (Barry, 1991, 1992). Also, information regarding the activation pattern of muscle motor units at different levels of voluntary isometric contraction has been obtained via spectral analysis of recorded muscle sounds (Orizio et al., 1990).

Studies of frog skeletal muscle in vitro have revealed that, during isometric contraction, small lateral muscle movements produce pressure waves that correspond to muscle sounds (Barry, 1987; Frangioni, 1987). The pressure field generated by the lateral movements has been described by fluid mechanics equations for a vibrating sphere or short cylinder (Barry and Cole, 1988). The predictions of the equations were verified experimentally, revealing that the pressure amplitude is directly proportional to, and in phase with, the lateral acceleration of the muscle (Barry and Cole, 1988). The lateral muscle movement occurs in an oscillatory manner, producing sounds with frequencies that equal the muscle's mechanical transverse resonant frequencies (Barry and Cole, 1988, 1990; Dobrunz et al., 1990). The transverse mechanical resonant frequency, hereafter called resonant frequency, should not be confused with longitudinal resonant frequency, which refers to oscillating compressional waves that propagate along the longitudinal axis of the muscle with a natural period of vibration. The resonant frequency of a muscle is a function of several parameters of the muscle: length, mass, topology, the elastic modulus ($E_b$) that resists lateral bending, tension, and fluid medium. Of these parameters, only muscle $E_b$ and tension may change significantly during isometric contraction. During isometric contractions of frog skeletal muscles, two hypotheses were tested: 1) temporal changes in muscle resonant frequency are dependent primarily upon changes in muscle tension and $E_b$; and 2) if muscle resonant frequency, tension, mass, length, topology, and fluid medium density are known, the $E_b$ can be determined by the equations that describe vibrations of beams subjected to tensile forces.

## METHODS

Whole frog (Rana pipiens) semitendinosus (STD) and gastrocnemius (GTN) muscles were isolated and removed from cold-anesthetized animals. The tendon from one end of each muscle was sutured to the steel hook of a tension transducer (model F5A-1; compliance of 2.0 $\mu$m/N; Konigsberg Instruments, Inc., Pasadena, CA), leaving as little tendon as possible between the tie and the hook. The other tendon of each muscle was tied directly to the arm of a stiff servomotor (model 305; Cambridge Technology, Inc., Watertown, MA) or a fixed post. Each muscle was suspended between the tension transducer and servomotor or fixed post, and placed in a bath of frog Ringer's solution (115 mM NaCl, 2.5 mM KCl, 1.8 mM $CaCl_2$, 2.15 mM $Na_2HPO_4$, 0.85 mM $NaH_2PO_4$) (Julian and Morgan, 1979) and held at

*Received for publication 22 March 1993 and in final form 28 January 1994.*

Address reprint requests to Neil M. Cole, Institute of Gerontology, Room 960, University of Michigan, 300 North Ingalls, Ann Arbor, MI 48109-2007. Tel.: 313-936-2102; Fax: 313-936-2116.

© 1994 by the Biophysical Society

0006-3495/94/04/1104/11 $2.00

10.3–11.6°C. The servomotor system has low compliance (2.0 μm/N) in steady-state conditions, but is more compliant to rapid changes in tension. To reduce the compliance, a feedback circuit was utilized to improve the servomotor's ability to maintain constant muscle length during tension transients. The circuit differentiates an amplified tension signal from the Konigsberg tension transducer and feeds it into the position control of the servomotor. The circuit can be adjusted to condition the differentiated signal to optimize the reduction in servomotor compliance during transient changes in tension. The movement of the arm due to transient tensional loads from contracting frog skeletal muscle is reduced to less than ±3 μm for muscle tension transients up to 3 Newtons.

Two hydrophones (model 8103; Bruel and Kjaer Instruments, Inc., Marlboro, MA) were used to provide an active hydrophone and a distant reference hydrophone for differential acoustic recording. Both hydrophones were calibrated and had a frequency response flat to ±1 dB over a range of 1.0 Hz to 30.0 kHz. The hydrophone signals were amplified and band-pass filtered from 2.0 Hz to 10.0 kHz by charge amplifiers (model 2635; Bruel and Kjaer), and then were differentially amplified and low-pass filtered at 2.0 kHz (model 8875A; Hewlett-Packard, Inc., Mountain View, CA).

Muscle contraction was induced via field stimulation created by current pulses transmitted across two platinum electrodes placed on either side of the muscle. Stimulation pulses were generated by a stimulator (model S88; Grass Instrument Co., Quincy, MA) and amplified by a power amplifier (model 275; Southwest Technical Products Corporation, San Antonio, TX). To reduce stimulation leakage currents that cause acoustic, tension, and muscle length signal distortion, the power amplifier was isolated from the rest of the system by placing a stimulation isolation unit (model SUI-5; Grass) between the stimulator and power amplifier. The power amplifier was powered via a one-to-one, 115 volt, 50–60 Hz, isolation transformer (model GIS-150; Stancor, United Technologies, Logansport, IN). Due to large current pulses required for stimulation, tetanic stimulation produced artifactual spikes in the acoustic record although the power amplifier was isolated. To remove the artifact, inverted stimulus pulses were added to the differential acoustic signal with an amplification needed to cancel the stimulus noise. To achieve adequate amplification the stimulation pulses were passively attenuated (model 350D; Hewlett-Packard, Inc., Mountain View, CA) and then filtered and selectively amplified (model 8875A; Hewlett-Packard).

Stimulation voltage was set slightly above the level at which maximal twitch tension is attained. The muscle length was then adjusted to $L_0$, the length at which the twitch tension was maximum. Optimum fiber length ($L_f$) was determined for each STD muscle by multiplying the $L_0$ by a previously determined fiber length to muscle length ratio of 0.63 (Faulkner et al., 1982). Tetanic stimulation was performed at 160 Hz. $P_0$ was defined as the maximum isometric tetanic force at $L_0$. The mean cross-sectional area of each muscle was estimated by dividing the muscle wet mass by the product of $L_f$ and 1060 kg/m$^3$, the density of mammalian muscle (Hill, 1932). Specific tension (kN/m$^2$) was estimated by dividing muscle tension by mean cross-sectional area. Length changes were imposed on the muscle at optimal length via the servomotor. Tension, length, and acoustic signals were recorded digitally using 12-bit analog-to-digital conversion with a 0.14 ms sampling rate for each signal.

### *Direct measurements of muscle longitudinal elastic modulus*

Longitudinal stiffness, $S_L$, was determined for STD muscles by imposing small sinusoidal length changes on each muscle at frequencies of 300 to 715 Hz. Oscillations of magnitude less than 0.1% $L_0$ were used to preserve the attachment of cross-bridge structures during muscle contraction (Halpern and Alpert, 1971). Recordings of changes in muscle length and tension development due to imposed length oscillations were obtained during tetanic contractions. $S_L$ was calculated and expressed as the longitudinal modulus of elasticity, $E_L$. $E_L$ is $S_L$ normalized for the length and cross-sectional area of the muscle.

$$E_L = \frac{\sigma}{\epsilon} = \frac{\Delta T/A}{\Delta L/L} = S_L \frac{L}{A} \quad (1)$$

where $L$ = muscle length, $E_L$ = longitudinal elastic modulus in N/m$^2$, $\sigma$ = stress in N/m$^2$, $\epsilon$ = strain in m/m, $T$ = tension in Newtons, $A$ = area in m$^2$, and $S_L$ = longitudinal stiffness in N/m. Functions of $E_L$ versus time were obtained for each STD muscle.

The tension output of the Konigsberg transducer has a resonant frequency of 8.13 kHz when clamped to the apparatus and immersed in water. The entire apparatus used to support the muscle during experimentation has several modes of resonance with the lowest at 40 Hz. To ensure that none of these modes were significantly excited by the muscle or servomotor during experimental procedures, system vibration was monitored by a pair of accelerometers and/or hydrophones attached to the apparatus on either side of the muscle in various configurations. Because of the large mass of the system, no vibration or acoustic energy above background noise was observed during isometric muscle activation. The largest vibrations detected occurred during imposed length oscillations via the servo-system. These vibrations were directed along the longitudinal axis of the muscle at a frequency equivalent to the servo-system oscillation frequency with an amplitude always less than 0.25 μm. Furthermore, the supports for the ends of the muscle were in phase during the vibration, thus, reducing the amplitude of muscle length changes due to system vibration to much less than 0.25 μm.

## Analytical methods

A mathematical prediction of the relationships among muscle resonant frequency, elastic modulus, and tension was derived by the Rayleigh energy method. A measure of muscle resonant frequency is provided by the time-varying dominant frequency of an acoustic signal produced during the rising phase of an isometric contraction. A temporal mapping of the resonant frequency is extracted from the acoustic signal by using a time-frequency transform, such as the Wigner distribution.

### *Calculation of muscle resonant frequency*

The acoustic signals obtained in this study are monocomponent in nature with a frequency that monotonically rises in time. Such signals are nonstationary and may be analyzed with time-frequency distributions. The Wigner distribution (WD), Eqs. 2 and 3, was chosen as an analytical tool for this study because it provides optimal time and frequency space resolution with minimal cross-term production for monocomponent and monotonic signals (Boashash and Black, 1987; Cohen, 1966, 1989; Wigner, 1932).

$$W(t, \omega) = \int_{-\infty}^{\infty} f(t + \tau/2) f^*(t - \tau/2) e^{-j\omega\tau} \, d\tau \quad (2)$$

where $t$ = time, $\omega$ = frequency, $f$ = signal, $\tau$ = a constant of integration, and * denotes complex conjugate.
In discrete form

$$W(n, \theta) = 2 \sum_{\tau=-\infty}^{\infty} e^{-2j\theta\tau} f(n + \tau) f^*(n - \tau) \quad (3)$$

where $n$ = discrete time, $\theta$ = discrete frequency.

WDs were calculated for the analytical forms of acoustic signal waveforms. Each acoustic waveform was sampled every 0.14 ms for 4096 points (573.44 ms). To reduce computation time, a 128 point subarray of the acoustic waveform was used to calculate the WD. The 128-point subarray was created by sampling every sixth point of the first 768 points (107.52 ms) of each acoustic array. The chosen sampling rate and array length resulted in temporal and frequency resolutions of 0.84 ms and 9.3 Hz, respectively. These resolution parameters produced "stair-like" data arrays with incremental steps 9.3 Hz high. Points between successive step rises in frequency were linearly interpolated for smoother graphical illustration. Because there was no significant acoustic power above 400 Hz, the resulting sampling frequency of 1190 Hz was still adequate.

The WD of an acoustic signal yields a two-dimensional time-frequency distribution (see Results). A time-function of the muscle's resonant frequency was obtained by reducing the two-dimensional distribution to a one-dimensional mapping of peak frequency versus time of contraction (Barry and Cole, 1990). At most points of time, a single peak dominates the WD of the acoustic waveform. During some parts of the waveform, secondary peaks may become significant due to cross-terms or because the acoustic signal becomes small. Furthermore, because discrete-time signals are periodic in both time and frequency domains, edge effects can result from a discontinuity between the beginning and end of the waveform. At very early or very late times these edge effects may distort the spectra. Nevertheless, the original peak is easily followed through most of the signal even when it is no longer the largest peak.

## Calculation of muscle tension with resonant frequency

**The Rayleigh method.** The relationship among muscle resonant frequency, measured via WDs of acoustic signals, and muscle $E_b$ and tension, was predicted by the Rayleigh method. The muscle was assumed to be simply supported because the ends of the muscle are free to pivot at their points of attachment. The density, length, and radial geometry were chosen to best approximate the properties of the muscles used in actual experiments. For small harmonic lateral deflections, as is the case with isometrically contracting muscles, the fundamental frequency can be expressed as

$$f^2(t) = \frac{E_b(t)\int_0^L I(x)\left[\frac{d^2y(x,t)}{dx^2}\right]^2 dx + T(t)\int_0^L -y(x,t)\left[\frac{d^2y(x,t)}{dx^2}\right] dx}{4\pi^2\rho_m(1+\epsilon)\int_0^L A(x)y^2(x,t)\,dx} \quad (4)$$

where the variables used are as follows:

$f$ = fundamental frequency in Hz. $t$ = time in ms.

$E_b$ = elastic modulus of the bending rigidity term, $E_bI(x)$, for whole muscle in N/m$^2$ (not the same as $E_L$ for whole muscle and fibrous steel cables).

$L$ = muscle length in meters. $I = \pi R^4/4$ = moment of inertia (area) in m$^4$.

$R$ = assumed cylindrical radius of muscle in meters.

$x$ = axial distance measured from one end of the muscle, expressed in m.

$y$ = muscle transverse deflection, expressed in m.

$T$ = longitudinal tension in Newtons. $\rho_m$ = muscle density is 1060 kg/m$^3$ (Hill, 1932).

$\epsilon = Am_f/m_m$ = added mass term for fluid kinetic energy, expressed as a fraction of muscle mass.

$A = \pi R^2$ = cross-sectional area of muscle in m$^2$. $m_m$ = muscle mass in kg.

$Am_f$ = apparent mass of fluid set in motion by muscle vibration, expressed in kg.

By solving for $T(t)$, tension can be written as the dependent variable, where

$$T(t) = \frac{4\pi^2\rho_m(1+\epsilon)f^2(t)\int_0^L A(x)y^2(x,t)\,dx - E_b(t)\int_0^L I(x)\left[\frac{d^2y(x,t)}{dx^2}\right]^2 dx}{\int_0^L -y(x,t)\left[\frac{d^2y(x,t)}{dx^2}\right] dx} \quad (5)$$

Muscle tension was calculated for each of the 128 resonant frequency time points calculated by the WD of each acoustic signal. For the numerical calculation, $y(x)$, $A(x)$, and $I(x)$ were divided into 512 intervals. See Appendix A for the derivation of Eq. 4 and the experimental and theoretical determination of the apparent mass of the fluid kinetic energy,

$$\epsilon\rho_m\int_0^L A(x)\,dx$$

where the fractions $\epsilon_{STD} \approx 0.67$ and $\epsilon_{GTN} \approx 0.64$.

**Mode Shape.** The solution to the Rayleigh expression, Eq. 4, is dependent on the relative shape of the muscle's modal deflection curve, $y(x, t)$, but is insensitive to its absolute magnitude. The muscle's static deflection curve was used as a substitute for $y(x, t)$, because it provides a good approximation to the relative shape of $y(x, t)$. The static deflection curve was calculated for the time-varying values of tension and $E_b$ during muscle contraction. Equation 6 describes the small static deflection of a muscle, $y(x, t)$ with a mass load per unit length, $-q(x)$.

$$\frac{d^2}{dx^2}\left[E_b(t)I(x)\frac{d^2y(x,t)}{dx^2}\right] - \frac{d}{dx}\left[T(t)\frac{dy(x,t)}{dx}\right] = -q(x) \quad (6)$$

where $q(x) = \rho_m\pi R^2(x)$ with $q(x)$ in kg/m (Crandall et al., 1978).

Muscles are assumed to be simply supported with boundary conditions:

$$y(0, t) = y(L, t) = 0$$

and

$$M = E_b(t)I(x)\frac{d^2y(x,t)}{dx^2} = 0 \quad \text{for } x = 0 \text{ and } x = L,$$

(Popov, 1968; Tse et al., 1978). Equation 6 reduces to

$$E_b(t)I(x)\left[\frac{d^2y(x,t)}{dx^2}\right] - T(t)y(x,t) = -\int_0^x\int_0^\beta q(\alpha)\,d\alpha\,d\beta + \left[\frac{x}{L}\right]\int_0^L\int_0^\beta q(\alpha)\,d\alpha\,d\beta \quad (7)$$

where, $\alpha$ and $\beta$ are constants of integration.

The modal deflection curve, $y(x, t)$, was obtained numerically from Eq. 7 by an iterative finite-difference method for second-order differential equations (Na, 1979). The range of $x$ was divided into 512 intervals for the numerical calculation. The $y(x, t)$ curve was calculated for 128 time points of muscle tension that correspond to the 128 points of muscle resonant frequency calculated using the WD. Note, the actual deflection of the muscle must be small compared to the muscle length. This restriction is primarily due to approximations used to obtain Eq. 4. See Appendix A for more details on the Rayleigh method.

**Calculation of $A(x)$ and $R(x)$.** Muscles were assumed to be tapered cylinders with radius $R(x)$. Muscle cross-sectional area, $A(x)$, was calculated as $\pi R^2(x)$. $R(x)$ was determined from 35 mm photographic prints of STD and GTN muscles held at $L_0$ in a passive state. The prints were obtained from two separate orthogonal views, each perpendicular to the longitudinal axis of each muscle. A 512 point digitized mapping of $R(x)$ for each print was measured. The respective mappings of R(x) obtained from the two orthogonal views for the STD and GTN muscles were averaged and defined as radial templates $\kappa_s(x)$ and $\kappa_g(x)$, respectively. The measures of $\kappa(x)$ for the two types of muscle were then used as templates for determining $R(x)$ of muscles used from other frogs of similar size. By scaling $\kappa(x)$ via the length and mass of each individual muscle, an approximate measure of $R(x)$ can be obtained for that particular muscle to be used in the Rayleigh approximation. For a cylindrical muscle, its mass and geometry can be related as follows:

$$\int_0^L \rho_m\pi R^2(x)\,dx = m_m \quad (8)$$

If we let

$$R(x) = c\kappa(x) \quad (9)$$

where $c$ is a constant scaling factor, and $\kappa(x)$ is the radial template for the muscle, then

$$R^2(x) = c^2\kappa^2(x).$$

By substitution,

$$\int_0^L \rho_m \pi c^2 \kappa^2(x)\, dx = m_m$$

solving for $c^2$,

$$c^2 = \frac{m_m}{\int_0^L \rho_m \pi \kappa^2(x)\, dx} \tag{10}$$

## RESULTS

Fig. 1 *a* shows the rising phase of tension produced by a tetanic contraction of a STD muscle while small sinusoidal length oscillations of 504 Hz, as determined by discrete Fourier transformation (Fig. 1 *b*) were imposed on the muscle. The peak-to-peak amplitude of the length oscillations were less than 0.1% of $L_0$, where $L_o$ = 25 mm and muscle mass = 0.059 g. The resulting $E_L$ measurement (Fig. 1 *c*) has a peak tetanic value of $3.65 \times 10^7$ N/m$^2$. Fig. 1 *d* shows tension and $E_L$ signals where their peaks were normalized to one and base levels normalized to zero. Tetanic tension (Fig. 1 *d*) was obtained by digitally low-pass filtering the signal in Fig. 1 *a* at 100 Hz to remove the superimposed oscillations before normalization. Because the frequency components contained in the tetanic tension signal and the frequency of oscillation are adequately separated, the oscillations were removed with no significant distortion of the tension signal. This was proved by observing that the filtered tension signal was graphically indistinguishable from an unfiltered tension signal without superimposed oscillations. Observation of Fig. 1 *d* indicates that, during the rising phase of tension development, $E_L$ leads tension. The viscoelastic nature of frog STD muscle is demonstrated in Fig. 2, where the mean $E_L$ for 13 muscles is plotted as a function of frequency of length oscillation. Two exponential curves are displayed in Fig. 2. One curve corresponds to peak tetanic values of $E_L$, and the other displays values of $E_L$ calculated when muscle tension reaches 40% of $P_0$.

Fig. 3 *a* shows an acoustic waveform obtained from an isometric tetanic contraction of a GTN muscle held at $L_0$ with the hydrophone positioned to record the major mode of lateral muscle vibration. The WD was utilized to obtain a two-dimensional time-frequency mapping of the acoustic signal. The two-dimensional distribution was simplified by multiplying the distribution by a simple time-frequency mask. The mask was equal to one at the peak frequency at each discrete moment in time and zero elsewhere. The masking allowed the reduction of the data to a one-dimensional representation of peak frequency vs. time of contraction (Fig. 3 *b*). Because, at the onset of contraction, the original acoustic signal displays a very sharp rise extending from a flat signal before contraction, acting similar to a discontinuity, a wide band of frequencies is observed early in the signal. The wide band makes it difficult to extract a single dominant resonant mode early in contraction. To reduce the effects of the pseudo-discontinuity, a single cycle of a low frequency sine wave with rising amplitude was spliced into the signal just before the sharp rise (Fig. 3 *a*). The splicing of the sine wave has a smoothing effect that sharpens the distribution of frequencies early in the signal, making it easier to extract a dominant

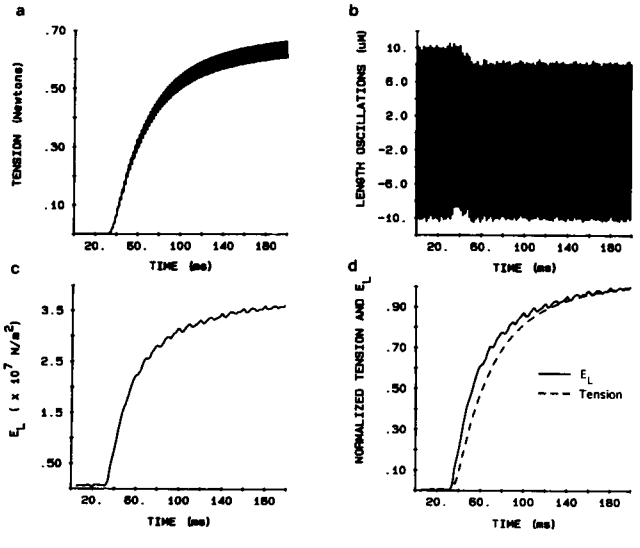


FIGURE 1 Data obtained from the early phase of a tetanic contraction with small length oscillations imposed on a muscle held near $L_0$ = 25 mm. (*a*) Tension with superimposed oscillations. (*b*) Length oscillations. (*c*) longitudinal elastic modulus, $E_L$. (*d*) Comparison of $E_L$ (*solid line*) and tension (*dashed line*) where their peaks were normalized to one and base levels normalized to zero. The tension in *d* was obtained by frequency filtering the tension signal shown in *a* to remove the imposed oscillations. Comparison to a tension trace without imposed oscillations showed that the filter produced neither distortion of the tension waveform nor a significant shift in time. The muscle was held at 10.8 ± 0.5°C, mean ± sample SD.

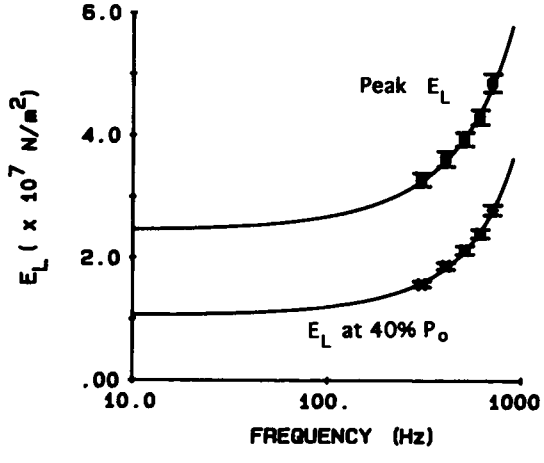


FIGURE 2 $E_L$ plotted as a function of length oscillation frequency. Data points (mean ± SE, $n$ = 13) are given for oscillation frequencies of 304 ± 4 Hz, 406 ± 5 Hz[1], 508 ± 5 Hz, 610 ± 3 Hz, 707 ± 6 Hz (mean ± SD) calculated with the discrete Fourier transform. Exponential curves were fit to the data points where $y = \exp(ax + b) \times 10^7$ N/m$^2$. The top curve, symbol "O", corresponds to peak tetanic $E_L$ with $a$ = 0.00096 and $b$ = 0.89322. The bottom curve, symbol "*", represents $E_L$ data measured at 40% maximum tetanic tension with $a$ = 0.00137 and $b$ = 0.05839. Vertical line at 150 Hz.
[1]indicates $n$ = 12.

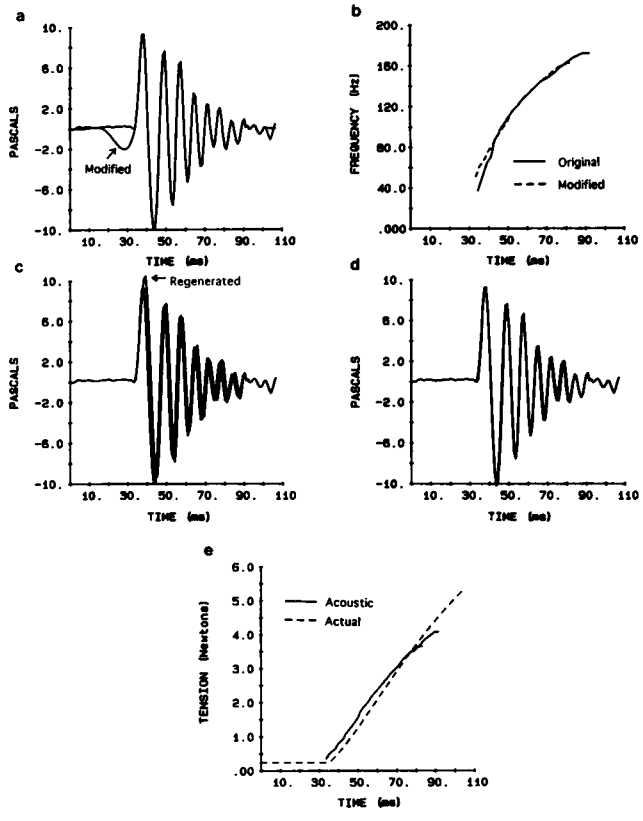


FIGURE 3 (*a*) The original and modified (*arrow*) acoustic signals obtained from a single isometric tetanic contraction of a frog GTN muscle held at $L_0$. The modified signal is generated by inserting a single-cycle sine wave with increasing amplitude before the initial rise of the signal. The inserted sine wave has a period 5 times longer than the first half-cycle of the acoustic signal. Furthermore, the slope of the end of the inserted sinusoid was matched to the slope of initial rise of the acoustic signal by adjusting the rate of increase of the amplitude of the inserted sine wave. Also, the very last half-cycle of the signal, which is noisy and has an amplitude much greater than the previous half-cycle, is reduced to zero to equate the endpoints. (*b*) Peak modal frequencies calculated from the WDs of the original and modified (- - - -) acoustic signals in *a*. (*c*) Comparison of the original acoustic signal with the regenerated form of the signal (*arrow*) using the peak frequencies, shown in *b* (*solid*), calculated from the original acoustic signal. (*d*) Comparison as in *c*, except that the peak frequencies, shown in *b*(- - - -) with arrow, were calculated using the modified form of the acoustic signal. (*e*) Comparison of tension measured via the tension transducer (- - - -) and the tension calculated using the peak acoustic frequencies and the Rayleigh method, with $E_b$ = 0 N/m$^2$. For the acoustic measures of tension, the portion of the curve indicated with the bracket is calculated using the original acoustic signal while the rest is calculated from the preconditioned signal. The two curves overlap. Muscle mass = 0.496 g, $L_0$ = 3.5 cm, Temperature = 11.6°C.

mode. The peak frequencies (Fig. 3 *b*) accurately trace the dominant mode of the time-frequency distributions of the signals in Fig. 3 *a* until the effects of small acoustic signal amplitude and low frequency cross-terms disrupt the calculation. By implementation of the mask and a synthesis procedure, the original acoustic signal was reconstructed from the dominant modal frequencies present in the distribution to demonstrate the power of the WD. The signal was reconstructed using a temporal array of peak frequencies, $f(t)$, calculated via the WD. The reconstruction was performed by integrating $2\pi f(t)$ to obtain the phase, calculating the sine of the phase, and multiplying the resulting sinusoid by the magnitude envelope of the analytical form of the original signal. Fig. 3, *c* and *d*, shows comparisons of the original acoustic signal and the reconstructed signals. The reconstruction using peak modal frequencies from the modified signal via sine splicing (Fig. 3 *d*) is nearly identical to the original, whereas the "unconditioned" signal starts lagging the original early in the signal (Fig. 3 *c*). Fig. 3 *e* shows a comparison of the tension measured via the Konigsberg tension transducer and that calculated using the acoustic frequencies in Fig. 3 *b* and the Rayleigh method described in Methods with $E_b$ set to 0 N/m$^2$, assuming $E_b$ makes a negligible contribution to muscle resonant frequency. With the assumption that $E_b$ is negligible, the Rayleigh method provides a very good approximation to the Konigsberg tension.

The results from an unfused tetanus at $L_0$ of the same muscle as in Fig. 3 are shown in Fig. 4. The muscle is subjected to two stimulus pulses. One pulse is applied while the muscle is in a passive state, and the other during the fall-off of the twitch-tension initiated by the first stimulus pulse. Two chirp-like signals appear in the acoustic signal (Fig. 4 *a*), each corresponding to a stimulus pulse. Fig. 4 *b* shows a comparison of the Konigsberg tension and the acoustically measured tension calculated using the peak acoustic frequencies from the two chirps, preconditioned as done for Fig. 3, and the Rayleigh method with $E_b$ = 0 N/m$^2$. The first acoustic signal provides a very good estimate of tension. The second chirp provides an estimate of tension that is initially below the Konigsberg measurement. Because the muscle is in a high tension state at the onset of the second chirp, its resonant frequency is quite high. This requires a step-like jump in muscle oscillation frequency to achieve resonant vibration. It takes about ¼ of an oscillation cycle for the

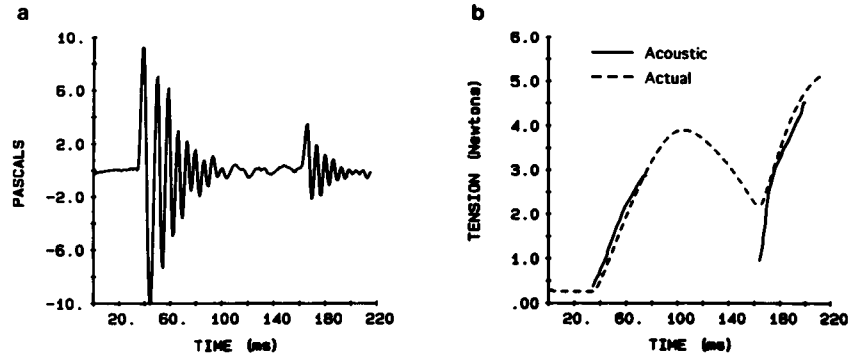


FIGURE 4 (*a*) Acoustic recording showing two chirp-like sounds generated from an unfused tetanus of the same muscle in Fig. 3. (*b*) Comparison of tension measured via the tension transducer (- - -) and the acoustic method using the modal frequencies calculated from the WDs of the two chirps in *a*, and $E_b$ = 0 N/m$^2$.

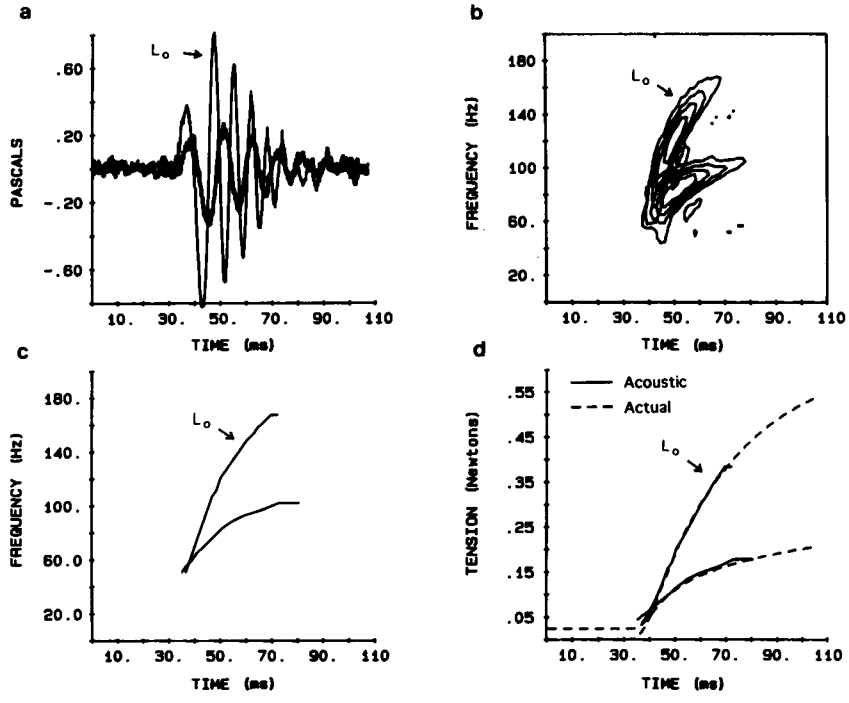


FIGURE 5 (*a*) Two overlaid acoustic signals recorded from isometric tetanic contractions of a single STD muscle held at $L_o$ (*arrow*) and 1.24 $L_0$. (*b*) Two overlaid WDs of the acoustic signals in *a*. (*c*) The peak modal frequencies of the two WDs in (*b*). The arrow indicates frequencies calculated for the sound recorded at $L_o$. (*d*) Comparison of tensions measured via a tension transducer (- - - -) and tensions calculated with the Rayleigh technique ($E_b$ = 0 N/m$^2$) using the acoustic measures of resonant frequency shown in *c*. Four curves are shown with the arrow indicating the two curves at $L_0$. For both lengths the acoustic and transducer curves are nearly indistinguishable. Muscle mass = 0.059 g, $L_0$ = 2.5 cm.

muscle to reach resonance, thus, producing the underestimation of tension. The initial portion of the acoustic signal is related to the driving mechanism that initiates the lateral motion of the muscle. The remainder of the signal is resonant vibration, where the acoustic estimate of tension continues to rise well above the first signal.

Fig. 5 *a* shows two overlaid acoustic signals from isometric tetanic contractions of a STD muscle at lengths of $L_0$ and 1.24 $L_0$. At 1.24 $L_0$ passive tension (0.024 N) is considerably higher, and the amplitude and frequencies of the muscle sound are much less than at $L_0$. The WD contour plot (Fig. 5 *b*) and the WD peak modal frequencies (Fig. 5 *c*) demonstrate the difference in the muscle's resonant frequencies at the different lengths. Because the initial rise of these acoustic signals was not as rapid as in the above GTN muscle, no preconditioning of the signals was necessary before applying the WD, other than that described in the Methods. Using the frequencies in Fig. 5 *c*, measures of tension were calculated for both lengths using the Rayleigh method with $E_b$ = 0 N/m$^2$, and plotted with Konigsberg tension (Fig. 5 *d*). For both lengths, the acoustic and Konigsberg measured tension provide for nearly a perfect match.

Fig. 6 shows a comparison of acoustic and Konigsberg measured tetanic specific tension averaged for 13 whole STD muscles held at $L_0$ and a temperature of 10.7 ± 0.4°C (mean ± SD). Assuming $E_b$ contributes negligibly to muscle transverse resonant frequency, acoustic tension was determined using the Rayleigh method with $E_b$ set to 0 N/m$^2$. No significant difference is observed between the two curves except for very early in the signal. The equality of acoustic and Konigsberg measured tension indicates that the temporal variation of the resonant frequency of an isometrically contracting STD muscle is primarily dependent on muscle tension. The contribution of elastic modulus is negligible throughout most of the signal except for a possible contribution near the onset of the rise in tension. The specific $P_0$ measured for the 13 muscles in Fig. 6 was 204 ± 5 kN/m$^2$ (mean ± SE). This value compares with 206 ± 22 kN/m$^2$ (mean ± SE) measured at 20°C for five whole STD muscles from frog Rana pipiens (Faulkner et al., 1982) and 223 ± 12 kN/m$^2$ (mean ± SE) at 2°C for seven intact STD fibers from frog Rana temporaria (Edman, 1979).

The dependence of acoustic estimates of muscle tension, $T$, on $E_b$, is shown in Fig. 7. A curve is displayed of $T(E_b)$ as a percentage of $T(E_b = 0)$. $T(E_b)$ is calculated for values of $E_b$ set to elastic modulus values ranging from 0 to 5.0 × 10$^7$ N/m$^2$, and resonant frequencies obtained experimentally when muscle tension is 0.4 $P_0$. Any deviation in the curve from approximately 100% indicates a deviation from the actual tension produced by the muscle, because $T(E_b = 0)$ is essentially equivalent to the tension measured by the tension transducer (Fig. 6). The two vertical lines indicate $E_L$ values corresponding to 40% maximum tetanic tension and 150 Hz length oscillations. The far right vertical line, $E_L$ = 1.3 × 10$^7$ N/m$^2$, was obtained from Fig. 2. The left vertical line, $E_L$ = 4.6 × 10$^6$ N/m$^2$, was obtained by extrapolation from data on frog sartorius muscle published by Halpern and Moss (1976).

## DISCUSSION

Theories of elastic beam behavior predict that the frequency of lateral resonant vibration of a beam is a function of both elastic modulus and tension. Standard elastic beam equations are ordinarily derived with the simplifying assumption that the beam is homogeneous and isotropic, thus equating $E_b$ and

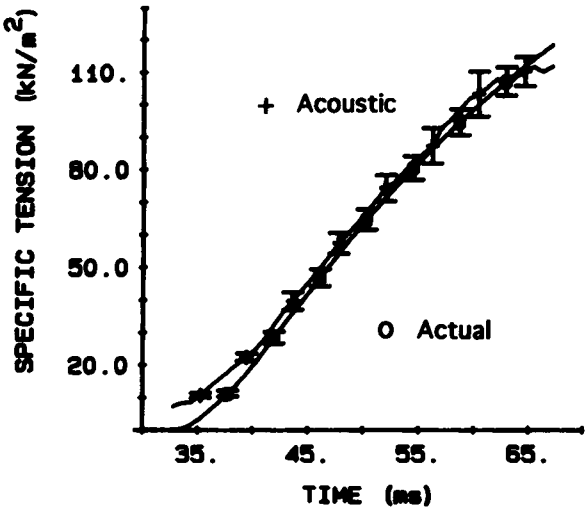


FIGURE 6 Comparison of specific tensions (mean ± SE) measured via the tension transducer, symbols "O", and specific tensions using the Rayleigh method ($E_b$ = 0 N/m$^2$) in conjunction with acoustic measures of muscle resonant frequency, symbols "+". Data obtained from 13 STD muscles, each tetanically contracted at $L_0$ and held at 10.7 ± 0.5°C (mean ± SD). With $n$ = 13 and values listed as mean ± SD, muscle $P_0$ = 204 ± 19 kN/m$^2$, muscle length = 0.024 ± 0.0012 m, muscle mass = 0.057 ± 0.0079 g.

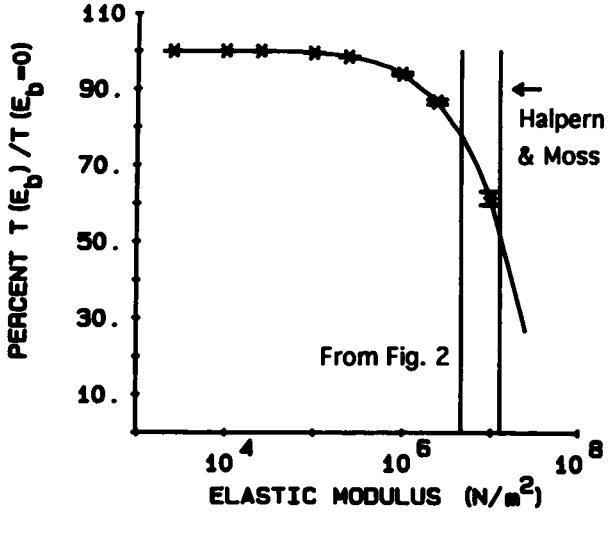


FIGURE 7 Plot of dependence of acoustically calculated tension (mean ± SE) on $E_b$ for the 13 muscles used to obtain Figs. 2 and 6. Acoustic values of tension were calculated at 40% maximum tetanic tension. Vertical lines indicate direct longitudinal measures of $E_L$ corresponding to 150 Hz length oscillations and 40% maximum tetanic tension. Arrow indicates vertical line corresponding to data from Fig. 2, $E_L = 1.3 \times 10^7$ N/m$^2$ = $10^{7.1}$ N/m$^2$. The other vertical line, $E_L = 4.6 \times 10^6$ N/m$^2$ = $10^{6.7}$ N/m$^2$, was obtained via extrapolation from data by Halpern and Moss (1976).

$E_L$. The substitution of direct measures of $E_L$ for $E_b$ indicates that for whole skeletal muscles, assumptions of homogeneity and isotropic behavior produce large discrepancies in the relationships among muscle resonant frequency, elastic modulus, and tension. Because of its internal fibrous structural composition, whole skeletal muscle is inherently non-homogeneous and anisotropic. Consequently, for this study one must distinguish between values of $E_b$ and $E_L$ (see Appendix B).

As a result of our inability to measure $E_b$ directly, the relationship between muscle resonant frequency and tension was initially explored under the assumption that the influence of $E_b$ on the mechanical vibration of skeletal muscle is negligible. With $E_b$ set to zero, estimates of muscle tension calculated via the acoustic method were nearly indistinguishable from direct measures of muscle tension via the tension transducer for both frog GTN and STD muscles. Therefore, despite the structural differences in both fiber alignment and whole muscle geometry, analysis of both muscles demonstrated that tension is the primary modulator of muscle resonant frequency. Our analysis was unable to clearly detect the effects of $E_b$ on muscle resonant frequency except for a probable influence very early in the acoustic signal, where at very low tension, $E_b$ appears to significantly raise the muscle's resonant frequency. Therefore, although the effects of muscle tension dominate, our data supports our first hypothesis that changes in whole muscle resonant frequency during isometric contractions are dependent primarily upon changes in both muscle tension and $E_b$.

### *Estimating $E_b$*

Because of the inequality of $E_b$ and $E_L$ in whole muscle and the negligible influence of $E_b$ on resonant frequency, muscle sounds may be used to estimate muscle tension during the early phase of muscle excitation when muscles give rise to sounds, but are not a viable tool for measuring muscle stiffness. Due to the overwhelming dominance of the tension term in dictating muscle resonance, the actual value of muscle $E_b$ cannot be identified via the acoustic method. Our findings, therefore, do not support our second hypothesis. Nevertheless, an upper boundary can be assigned to $E_b$ where acoustic resonant frequency data exists. As an example, when the tension of the STD muscle is 40% of $P_0$, the actual value of $E_b$ is less than or equal to approximately $3 \times 10^5$ N/m$^2$, the value of $E_b$ in Fig. 7 where the curve begins to bend downward indicating a deviation in acoustically determined tension from direct measures of tension. This upper bound of $E_b$ is 43 times smaller than the corresponding value for $E_L$ of $1.3 \times 10^7$ N/m$^2$ determined at 40% of $P_0$. It is unlikely that the difference between $E_L$ and $E_b$ is due to poor measurements of $E_L$, because our values of $E_L$ are consistent with independently published results. Figs. 1 and 2 display stiffness results that are consistent with several previously completed tension-stiffness studies (Bagni et al., 1988; Cecchi, 1986; Hasan and Mason, 1978; Hatta et al., 1988; Mason, 1978; Schoenberg and Wells, 1984).

### *Comparison with earlier work*

The findings of the present study differ from previously published results. Dobrunz et al. (1990) reported that both elastic modulus and tension have a nearly equal contribution to

muscle resonant frequency of frog GTN muscle. The disparity between their results and those of the present study might be explained by some differences in methodology: 1) Dobrunz et al. (1990) used analytical solutions to their muscle model. The analytical approach required some simplifying assumptions, such as using a sinusoidal half-wavelength function as the mode shape of their muscle displacement. In the present study, numerical approaches allowed using the resting displacement of the muscle as the modal shape. Calculation of the resting displacement was based on the distribution of the mass and cross-sectional area projected along the longitudinal axis of the muscle. 2) The analytical Rayleigh calculations used uniform muscle cross-sectional area combined with a mass multiplied by 1.5 to correct for the spindle shape of the GTN muscle. The numerical methods in the present study allowed an approximation to the radial shape of the muscle to be directly incorporated into the calculations. 3) Consistent with the uniform muscle model, Dobrunz et al. (1990) corrected for fluid flow with an apparent mass equivalent to the mass of the fluid displaced by the muscle and a velocity equal to that of the muscle. This apparent mass was based on Lamb's (1932) finding for the fluid flowing around a long cylinder moving at right angles to its longitudinal axis. Due to the complex geometry of the muscles, however, and the fact that the muscles are bending rather than translating through the fluid, it is difficult to predict the apparent mass of the fluid set in motion by the muscles without experimentation. Theoretical predictions of the apparent mass of the fluid set in motion for a translating sphere and long cylinder are 0.5 and 1.0 times the mass of the fluid displaced by the objects, respectively. Because the muscles used in experimentation are spindle-shaped, the apparent mass of the fluid would be expected to fall between that of a long cylinder and a sphere. The experimentally measured value for the GTN was approximately 0.64 times the mass of the fluid displaced by the muscle. The value of 0.64 produces a lower measurement of the total vibrational kinetic energy due to muscle activity than predicted by the long cylinder model.

### *Summary*

We conclude that during supramaximum stimulation of isometric muscles, tension is the primary modulator of skeletal muscle resonant frequency and, thus, the acoustic signal frequency. Muscle $E_b$ has a negligible influence on muscle resonant frequency except for very early in activation where the frequency content of the acoustic signal is higher than predicted by the Rayleigh tension term. Because the effects of $E_b$ are minimal, acoustic measures of resonant frequency can be used to estimate changes in tension during the early phase of contraction. Furthermore, because muscles are comprised of numerous thin fibers, their elastic and resonant behavior is similar to a tensioned fibrous cable with distributed mass. Therefore, muscle sounds emitted during contraction reflect the fibrous composition of whole muscle and the inequality of $E_L$ and $E_b$. Because muscles are fibrous, it is unlikely that an increase in whole muscle radius-to-length ratio that falls within reasonable physiological and anatomical dimensions, would increase $E_b$ enough to produce a significant influence on muscle resonance (see Appendix B). Tension will likely dominate modulation of acoustic frequencies.

## APPENDIX A

## The Rayleigh method

Equations 4 and 5 in Methods were obtained via the Rayleigh method. The Rayleigh method provides a numerical approach for determining the fundamental frequency of systems that contain flexible elements that may be subjected to longitudinal tensile forces, such as strings, springs, cables, and beams. For computational purposes, muscles were assumed to have uniform density. The Rayleigh method is based on the principle of conservation of energy. For a system undergoing harmonic motion, maximum kinetic and maximum potential energies are equal. Both kinetic and potential energies are expressed in terms of the muscle's assumed deflection curve.

### *Potential energy*

The total maximum potential energy, $U_{max}$, of the muscle is equivalent to the addition of a bending component, $U_b$, and a longitudinal tension, $U_T$, component.

$$U_{max} = U_b + U_T \tag{A1}$$

where,

$$U_b = \frac{1}{2}\int_0^L E_b(x)I(x)\left[\frac{d^2y(x)}{dx^2}\right]^2 dx \tag{A2}$$

$$U_T = -\frac{1}{2}T\int_0^L y(x)\left[\frac{d^2y(x)}{dx^2}\right] dx \tag{A3}$$

and

$E_b(x)$ = elastic modulus of the bending rigidity term $E_bI(x)$ in N/m$^2$. As is discussed in the discussion section and Appendix B, whole muscle exhibits anisotropic behavior similar to a cable where $E_b \neq E_L$.

$I(x)$ = moment of inertia (area) in m$^4$.

$y(x)$ = the muscle deflection curve, normal to the longitudinal axis, $x$, of the muscle expressed in meters.

$T$ = muscle tension in Newtons. $L$ = muscle length, in meters.

For muscles with small deflections, less than 10 percent of the muscle's length, the maximum total potential energy, $U_{max}$, can be written as (Lamb, 1932; Popov, 1968; Thomson, 1981):

$$U_{max} = \frac{1}{2}\int_0^L E_b(x)I(x)\left[\frac{d^2y(x)}{dx^2}\right]^2 dx + \frac{1}{2}T\int_0^L - y(x)\left[\frac{d^2y(x)}{dx^2}\right] dx \tag{A4}$$

where $U_{max}$ is evaluated with the curve, $y(x)$, at its maximum deflection.

### *Kinetic energy*

The total maximum kinetic energy, $K_{max}$, is equivalent to the addition of the maximum kinetic energy of the moving muscle, $K_m$, and the maximum kinetic energy of the movement of the fluid medium surrounding the muscle, $K_f$. The maximum kinetic energy for the muscle is

$$K_m = \frac{1}{2}\omega^2\int_0^L y^2(x)\, d_{m_m} \tag{A5}$$

where $\omega$ = fundamental frequency in rad/s. $m_m$ = muscle mass in kg (Blevins, 1979; Thomson, 1981).

Because the muscle is vibrating in a fluid medium, and not a vacuum, the kinetic energy of the fluid medium due to muscle movement must be considered. The kinetic energy of the fluid has an apparent mass equivalent to a fraction of the fluid displaced by the muscle and a velocity equivalent to that of the muscle. A long cylinder with uniform radius moving at right angles to its longitudinal axis, has an apparent mass equivalent to the mass of the water displaced by the cylinder. A spherical object has an apparent mass equivalent to ½ the mass of the displaced water (Blevins, 1979). Because the muscle is a tapered cylinder, it can be expected to behave similar to an ellipsoid and have an apparent mass that falls between that of a sphere and a cylinder. Because the whole muscle, however, has a rather complex geometry and is bending rather than translating laterally as a whole, theoretical predictions of the apparent mass are unreliable. Therefore, direct measures of the fluid's apparent mass were obtained experimentally. Vibrations were recorded from passively plucked and stimulated GTN muscles both in Ringer solution (density ≈ 1005 kg/m$^3$ at 11°C) and in air (density ≈ 1.2 kg/m$^3$) (Blevins, 1979). GTN muscles were stimulated via a suction electrode attached to the severed sciatic nerve, rather than field electrodes, to enable stimulation in air. The difference in frequency of muscle vibration in air ($f_a$) and in fluid ($f_f$) was then used to calculate the apparent mass of the fluid kinetic energy, $Am_f$. Because air density, unlike fluid density, is nearly three orders of magnitude lower than muscle density, the contribution of air flow to the total kinetic energy as a result of muscle vibration is negligible and may be ignored.

$$Am_f = [(f_a/f_f)^2 - 1]m_m \tag{A6}$$

(Blevins, 1979).If we let $\epsilon = Am_f/m_m$, which is the added mass term expressed as a fraction of muscle mass, then

$$K_f = \frac{1}{2}\epsilon\omega^2 \int_0^L y^2(x)\, dm_m \tag{A7}$$

For STD muscles, direct experimental data were difficult to obtain. Because the nerve enters the muscle near the center of its belly, an attached suction electrode would distort lateral vibrations. Therefore, experimental data from GTN muscles were adapted to STD muscles using predictions from literature in the following manner. Predictions for the added masses of both GTN and STD muscles were calculated using predictions from an ellipsoid model (Blevins, 1979). The fraction obtained by dividing the predicted added mass for the STD by that predicted for the GTN was multiplied by the GTN experimental finding to obtain an approximation for the STD.

The maximum kinetic energy, $K_{max}$, may be expressed as

$$K_{max} = \frac{1}{2}(1 + \epsilon)\omega^2 \int_0^L y^2(x)\, dm_m \tag{A8}$$

when $K_{max}$ is evaluated with the curve, $y(x)$, at its maximum deflection. $\epsilon_{STD} \approx 0.67$ and $\epsilon_{GTN} \approx 0.64$.

### Rayleigh method

By equating $U_{max}$ and $K_{max}$, the following expression for the muscle's fundamental frequency is obtained.

$$\omega^2 = \frac{\displaystyle\int_0^L E_b(x)I(x)\left[\frac{d^2y(x)}{dx^2}\right]^2 dx + T\int_0^L -y(x)\left[\frac{d^2y(x)}{dx^2}\right] dx}{(1 + \epsilon)\displaystyle\int_0^L y^2(x)\, dm_m} \tag{A9}$$

(Thomson, 1981).

The muscle's mass, $m_m$, can be expressed as follows

$$m_m = \int_0^L \rho_m(x)A(x)\, dx \tag{A10}$$

where $\rho_m(x)$ is the muscle density along its longitudinal axis, expressed in kg/m$^3$. The density of the muscles used in this project is assumed uniform. Therefore, the muscle mass is

$$m_m = \rho_m \int_0^L A(x)\, dx \tag{A11}$$

It follows that

$$dm_m = \rho_m A(x)\, dx \tag{A12}$$

By substituting $2\pi f$ for $\omega$, where $f$ = the fundamental frequency in Hz, a uniform elastic modulus that changes in time $E(t)$ for $E(x)$, a tension that changes in time for, $T(t)$ for $T$, and Eq. A.12 into Eq. A.9, the following expression used for calculating fundamental frequencies through time is obtained:

$$f^2(t) = \frac{E_b(t)\displaystyle\int_0^L I(x)\left[\frac{d^2y(x,t)}{dx^2}\right]^2 dx + T(t)\int_0^L -y(x,t)\left[\frac{d^2y(x,t)}{dx^2}\right] dx}{4\pi^2\rho_m(1 + \epsilon)\displaystyle\int_0^L A(x)y^2(x,t)\, dx} \tag{A13}$$

The calculated value for $f(t)$ is dependent on the relative shape of the deflection curve $y(x, t)$, but is fairly insensitive to the absolute magnitude of the curve. If the exact value of $y(x, t)$ is assumed, the fundamental frequency obtained will be correct. In general, very accurate results can be obtained if the static deflection curve of the muscle is used for $y(x, t)$.

## APPENDIX B

## Elastic behavior of fibrous cables and whole muscles

The characteristic nonhomogeneous, anisotropic internal fibrous nature of whole skeletal muscle may explain the inequality of $E_b$ and $E_L$. Whole STD muscles are comprised of numerous muscle fibers that lie in parallel to one another along the longitudinal tension generating axis of the muscle. The fibrous composition of whole muscle is analogous to a cable containing hundreds of thin wires.

### Fibrous cable

Due to different internal stress/strain patterns caused by bending, the bending rigidity, $E_bI$, of the fibrous cable is much less than the solid cable. In spite of these differences, the solid and fibrous cables have $E_L$s that are equivalent, assuming they contain approximately the same cross-sectional area of elastic material. Furthermore, unlike the fibrous cable, $E_L$ and $E_b$ for the solid isotropic cable are equal (Blevins, 1979). The reason the bending rigidity of the fibrous cable is less than that of the solid cable, and thus, less than its own $E_L$, is explained as follows. The bending rigidity of a solid cable is

$$E_bI_{solid} = E_LI_{solid} = E_L\pi\frac{(R_{solid})^4}{4}$$

where $I_{solid}$ is the moment of inertia (area) of the cable and $R_{solid}$ is the radius of the solid cable.

The overall bending rigidity of the fibrous cable, assuming there is negligible interaction, such as friction between fibers, is the summation of the bending rigidity terms of each of the individual fibers (Blevins, 1979). The bending rigidity of the fibrous cable can be expressed as

$$\sum_n E_{bf}I_{fiber} = \sum_n E_LI_{fiber} = \sum_n E_L\pi\frac{(R_{fiber})^4}{4}$$

where $n$ is the number of fibers in the cable. $I_{fiber}$ is the moment of inertia (area) for the individual fibers. $R_{fiber}$ is the radius of each of the fibers, and,

$E_{bf}$, which is equivalent to $E_L$, is the elastic modulus of each of the fibers. If we assume the radii of all the fibers are equivalent, then the fibrous cable bending rigidity is

$$nE_L I_{fiber} = nE_L \pi \frac{(R_{fiber})^4}{4}$$

Because we have assumed that the total cross-sectional area of elastic material for each cable is equivalent, which is a reasonable approximation for cables with large $n$, it follows that

$$Area = \pi (R_{solid})^2 = n\pi(R_{fiber})^2$$

Therefore,

$$R_{fiber} = \frac{R_{solid}}{\sqrt{n}}$$

and

$$n = \left[\frac{R_{solid}}{R_{fiber}}\right]^2$$

It follows that the bending rigidity of the fibrous cable is

$$\frac{E_L \pi (R_{solid})^2 (R_{fiber})^2}{4} = \frac{E_L \pi (R_{solid})^4}{4n}$$

Therefore, the bending rigidity of the solid cable is $n$ times larger than the fibrous cable with the same $E_L$ and overall radius. It follows, that when viewing the fibrous cable as a whole, its $E_L$ is $n$ times greater than its overall $E_b$.

### *Skeletal muscle*

Now consider skeletal muscle. A difference of one to two orders of magnitude exists between the possible values of $E_b$, any value less than approximately $3 \times 10^5$ N/m$^2$ where the curve in Fig. 7 begins to roll downward, and our measure of $1.3 \times 10^7$ N/m$^2$ for $E_L$. Assuming an average radius of 59 $\mu$m for individual frog muscle fibers (Blinks, 1965; Edman and Hwang, 1977), a whole muscle of radius 0.84 mm, like the muscle used in Fig. 1, is comprised of approximately 200 parallel fibers as seen from a cross-sectional view. Such a muscle would have an $E_L$ 200 times larger than its $E_b$, if its fibers were homogeneous, isotropic, and acted independently during bending. In fact, muscle fibers are not homogeneous and are unlikely to be isotropic because of their longitudinally oriented myofilament composition. Such a composition is likely to cause a larger discrepancy between $E_L$ and $E_b$. Nevertheless, for simplicity we will assume the fibers are isotropic. The factor of 200 is large enough to account for the disparity between $E_b$ and $E_L$.

For whole STD muscles, the muscle fibers are not entirely independent of one another. As the muscle bends and the parallel fibers try to slide past one another, factors such as connective tissue and friction can cause interactions among adjacent fibers that resist bending. The interactions among fibers will increase the bending rigidity of the whole muscle beyond the simple summation of the bending rigidities of all the individual fibers. This interaction will tend to bring the measures of $E_b$ and $E_L$ of the whole muscle closer to one another. How much closer is a function of how freely adjacent fibers can slide longitudinally past one another during bending. Because the bending that occurs during sound production has a peak lateral deflection that is 70 to 80 times smaller than whole muscle length (Barry and Cole, 1988), and the average radius of individual fibers is only 59 $\mu$m, very small differentials are developed between strains of adjacent muscle fibers. Therefore, only a very minimal amount of low resistive sliding is necessary to allow independent bending of individual adjacent fibers as the whole muscle bends during sound production.

The compliance of the elastic connective tissues distributed between individual fibers allows a certain degree of freedom of motion between adjacent fibers (Bloom and Fawcett, 1986). Thus, the fibers can behave with some independence of their neighbors, enabling them to slide past one another over very short distances during the vibrational bending that initiates the production of sound. If the fibers have little resistive interaction to sliding during sound production, the fiber composition of muscle can fully account for the inequality of $E_b$ and $E_L$. Furthermore, for muscles with parallel fibers, the force of interaction is likely to remain nearly constant throughout the muscle contraction since the interaction is independent of the muscle contractile machinery. For muscles with pennate fiber architecture, the frictional force of fiber interaction may increase as muscle tension rises because their geometric orientation places them at an angle to the axis of whole muscle tension production, thus, producing increased lateral pressure between fibers.

### *Possible nonlinear elasticity may contribute to $E_L > E_b$*

Another possible contributor to the disparity between $E_L$ and $E_b$ is the existence of a nonlinear axial stress-strain relationship in skeletal muscle. The muscle may demonstrate stiffness measurements that differ for varying length perturbation amplitudes below 0.1% muscle length. For the lateral muscle vibrations that occur during sound generation, the axial strain is less than the axial strain induced during the direct sinusoidal measurement of muscle $E_L$. Peak-to-peak lateral deflection values of approximately 0.1 mm to 0.4 mm have been obtained during muscle sound production for a 30-mm-long muscle (Barry and Cole, 1988). Using these peak deflections, a deflection curve, $y(x)$, was calculated for typical STD muscles with $E_b$ set to $1 \times 10^6$ N/m$^2$ and a specific tension of $2.0 \times 10^5$ N/m$^2$. From the calculated deflection curve, axial strains of 0.003 to 0.045% muscle length were obtained. These axial strains produced during sound production are less than the strains of 0.08 to 0.1% used to measure $E_L$ during length perturbation experiments. If a nonlinearity in the stress-strain relationship of muscle exists between strains of 0.003 to 0.1% muscle length, then the elastic nonlinearity may contribute to the difference between $E_L$ and $E_b$.

We thank J. Faulkner, T. McMahon, N. Perkins, and W. Williams for helpful discussions. This work was supported by a grant from the National Science Foundation (BSC-9000257) to D. Barry.

## REFERENCES

Bagni, M. A., G. Cecchi, and M. Schoenberg. 1988. A model of force production that explains the lag between crossbridge attachment and force after electrical stimulation of striated muscle fibers. *Biophys. J.* 54:1105–1114.

Barry, D. T. 1987. Acoustic signals from frog skeletal muscle. *Biophys. J.* 51:769–773.

Barry, D. T. 1991. Muscle sounds from evoked twitches in the hand. *Arch. Phys. Med. Rehabil.* 72:573–575.

Barry, D. T. 1992. Vibrations and sounds from evoked muscle twitches. *Electromyogr. Clin. Neurophysiol.* 32:35–40.

Barry, D. T., and N. M. Cole. 1988. Fluid mechanics of muscle vibrations. *Biophys. J.* 53:899–905.

Barry, D. T., and N. M. Cole. 1990. Muscle sounds are emitted at the resonant frequencies of skeletal muscle. *IEEE J. of Biomedical Engineering* 37:525–531.

Barry, D. T., S. R. Geiringer, and R. D. Ball. 1985. Acoustic myography: a non-invasive monitor of muscle unit fatigue. *Muscle and Nerve.* 8:189–194.

Barry, D. T., J. A. Leonard, Jr., A. J. Gitter, and R. D. Ball. 1986. Acoustic myography as a control signal for an externally powered prosthesis. *Arch. Phys. Med. Rehabil.* 67:267–269.

Barry, D. T., K. E. Gordon, and G. G. Hinton. 1990. Acoustic and surface EMG diagnosis of pediatric muscle disease. *Muscle and Nerve* 13:286–290.

Barry, D. T., D. J. Im, and T. Hill. 1992. Muscle fatigue measured with evoked muscle vibrations. *Muscle and Nerve* 15:303–309.

Blevins, R. D. 1979. Formulas For Natural Frequency And Mode Shape. Van Nostrand Reinhold Company, New York. pp. 386–424.

Blinks, J. R. 1965. Influence of osmotic strength on cross-section and volume of isolated single muscle fibres. *J. Physiol.* 177:42–57.

Bloom, W., and D. W. Fawcett. 1986. A Textbook of Histology. 11th Ed. W. B. Saunders Company, Philadelphia. pp. 272–273.

Boashash, B., and P. J. Black. 1987. An efficient real-time implementation of the Wigner-Ville distribution. *IEEE Trans. Acoust., Speech, Signal Processing* 35:1611–1618.

Cecchi, G., P. J. Griffiths, and S. Taylor. 1986. Stiffness and force in activated frog skeletal muscle fibers. *Biophys. J.* 49:437–451.

Cohen, L. 1966. Generalized phase-space distribution functions. *J. Math. Phys.* 7:781–786.

Cohen, L. 1989. Time-frequency distributions. *IEEE Trans. Acoust. Sp. Sig. Proc.* 77:941–981.

Crandall, S. H., N. C. Dahl, and T. J. Lardner, editors. 1978. An Introduction to The Mechanics of Solids (second edition with SI units). McGraw-Hill Book Company, Incorporated, New York. pp. 577–589.

Dobrunz L. E., D. G. Pelletier, and T. A. McMahon. 1990. Muscle stiffness measured under conditions simulating natural sound production. *Biophys. J.* 58:557–565.

Edman, K. A. P. 1979. The velocity of unloaded shortening and its relation to sarcomere length and isometric force in vertebrate muscle fibers. *J. Physiol.* 291:143–159.

Edman, K. A. P., and J. C. Hwang. 1977. The force-velocity relationship in vertebrate muscle fibres at varied tonicity of the extracellular medium. *J. Physiol.* 269:255–272.

Faulkner, J. A., D. R. Claflin, K. K. McCully, and D. A. Jones. 1982. Contractile properties of bundles of fiber segments from skeletal muscles. *Am. J. Physiol.* 243(Cell Physiol. 12):C66–C73.

Frangioni, J. V., T. S. Kwan-Gett, L. E. Dobrunz, T. A. McMahon. 1987. The mechanism of low-frequency sound production in muscle. *Biophys. J.* 51:775–783.

Halpern, H., and N. R. Alpert. 1971. Special Communications. A stochastic signal method for measuring dynamic mechanical properties of muscle. *J. Appl. Physiol.* 31:913–925.

Halpern, W., and R. L. Moss. 1976. Elastic modulus and stress relationships in stretched and shortened frog sartorii. *Am. J. Physiol.* 230:205–210.

Hasan, H., and P. Mason. 1978. Pulse propagation in muscle. *Phys. Med. Biol.* 23:917–927.

Hatta, I., H. Sugi, and Y. Tamura. 1988. Stiffness changes in frog skeletal muscle during contraction recorded using ultrasonic waves. *J. Physiol.* 403:193–209.

Hill, A. V. 1932. Myothermic experience on the frog's gastrocnemius. *Proc. Roy. Soc. Bull.* 109:267–303.

Julian, F. J., and D. L. Morgan. 1979. Intersarcomere dynamics during fixed-end tetanic contractions of frog muscle fibers. *J. Physiol. (Lond.).* 293:365–378.

Lamb, H. 1932. Hydrodynamics. Dover, New York. p.77.

Mason, P. 1978. Dynamic stiffness and cross-bridge action in muscle. *Biophys. Struct. Mech.* 4:15–25.

Na, T. Y. 1979. Computational Methods In Engineering Boundary Value Problems. Academic Press, Inc., New York. pp. 93–136.

Orizio, C., R. Perini, and A. Veicsteinas. 1989. Changes of muscular sound during sustained isometric contraction to exhaustion. *J. Appl. Phys.* 66: 1593–1598.

Orizio, C., R. Perini, B. Diemont, N. M. Figini, and A. Veicsteinas. 1990. Spectral analysis of muscular sound during isometric contraction of biceps brachii. *J. Appl. Physiol.* 68:508–512.

Oster, G., and J. S. Jaffe. 1980. Low frequency sounds from sustained contraction of human skeletal muscle. *Biophys. J.* 30:119–127.

Popov, E. P. 1968. Introduction To Mechanics of Solids. Prentice-Hall, Englewood Cliffs, NJ. pp. 385–387.

Schoenberg, M., and J. B. Wells. 1984. Stiffness, force, and sarcomere shortening during a twitch in frog semitendinosus muscle bundles. *Biophys. J.* 45:389–397.

Thomson, W. T. 1981. Theory of Vibration With Applications. 2nd Ed. Prentice-Hall, Englewood Cliffs, NJ. pp. 210–213, 268–277.

Tse, F. S., I. E. Morse, and R. T. Hinkle. 1978. Mechanical Vibrations Theory and Applications. 2nd Ed. Allyn and Bacon, Inc., Boston, MA. pp. 253–271.

Wigner, E. P. 1932. On the quantum correction for thermodynamic equilibrium. *Physical Review.* 40:749–759.

Zwarts, M. J., and M. Keidel. 1991. Relationship between electrical and vibratory output of muscle during voluntary contraction and fatigue. *Muscle and Nerve.* 14:756–761.